YALE
PEABODY
MUSEUM

P.O. BOX 208118 | NEW HAVEN CT 06520-8118 USA | PEABODY.YALE. EDU

JOURNAL OF MARINE RESEARCH

The *Journal of Marine Research,* one of the oldest journals in American marine science, published important peer-reviewed original research on a broad array of topics in physical, biological, and chemical oceanography vital to the academic oceanographic community in the long and rich tradition of the Sears Foundation for Marine Research at Yale University.

An archive of all issues from 1937 to 2021 (Volume 1–79) are available through EliScholar, a digital platform for scholarly publishing provided by Yale University Library at https://elischolar.library.yale.edu/.

Requests for permission to clear rights for use of this content should be directed to the authors, their estates, or other representatives. The *Journal of Marine Research* has no contact information beyond the affiliations listed in the published articles. We ask that you provide attribution to the *Journal of Marine Research*.

Yale University provides access to these materials for educational and research purposes only. Copyright or other proprietary rights to content contained in this document may be held by individuals or entities other than, or in addition to, Yale University. You are solely responsible for determining the ownership of the copyright, and for obtaining permission for your intended use. Yale University makes no warranty that your distribution, reproduction, or other use of these materials will not infringe the rights of third parties.

This work is licensed under a Creative Commons Attribution-NonCommercial-ShareAlike 4.0 International License.
https://creativecommons.org/licenses/by-nc-sa/4.0/

Journal of Marine Research, 53, 249–267, 1995

Lateral entrainment in baroclinic currents II

by Melvin E. Stern[1] and Jean-Raymond Bidlot[2]

ABSTRACT

The strong mesoscale velocity fluctuations ("eddies") observed in the deep Gulf Stream region may be dynamically necessary to incorporate the Recirculation Gyres which account for the downstream increase in transport. The eddy-current interaction leading to entrainment is studied in a two layer quasi-geostrophic model with piecewise uniform potential vorticity. It is shown that the volume entrained by a bottom eddy of strength Γ_2^* initially located near the edge of a bottom current depends mainly on the lateral shear s_2 of this current, rather than on the much stronger shear of the upper layer. It is suggested that the "mean entrainment velocity" into an isopycnal layer of nearly uniform vertical thickness is proportional to $(\Gamma_2^* s_2)^{1/2}$, where Γ_2^* (cm^2/sec) is proportional to the integrated potential vorticity anomaly of the eddy.

1. Introduction

Although the large downstream increase in total Gulf Stream transport observed south and north of Cape Hatteras is eventually supplied by *mean* current inflows ("gyres") on either side (Hogg *et al.,* 1986) the much larger velocity fluctuations present in mesoscale eddies (Luyten, 1977) may be dynamically important in incorporating the gyre water across the stream's edge (Stern and Bidlot, 1994, hereafter cited as SB). In the latter paper the entrainment mechanism is discussed for a 1½ layer model, in which an upper eddy interacts with the upper stream flow, and in which the deep lower layer is stationary. But most of the observed increase in stream transport occurs in the lower layer, and therefore we shall now consider the full two layer entrainment problem in which the barotropic influence appears. This effect, considered previously in a *pure* barotropic model (Stern, 1991, hereafer S91), is summarized below because the barotropic component will be shown to be most relevant to entrainment in the present two layer quasi-geostrophic model.

The pure barotropic problem (Fig. 1) consists of a semi-infinite basic current with uniform cyclonic (+) vorticity $\bar{\zeta} = s_2$ on one side of an interface $y' = L\,(x', t)$, and irrotational ($\bar{\zeta} = 0$) fluid on the other side. In addition, the initial ($t = 0$) state

1. Florida State University, Department of Oceanography, Tallahassee, Florida, 32306-3048, U.S.A.
2. Management Unit of the Mathematical Model of the North Sea, 100 Gulledelle, 1200 Brussels, Belgium.

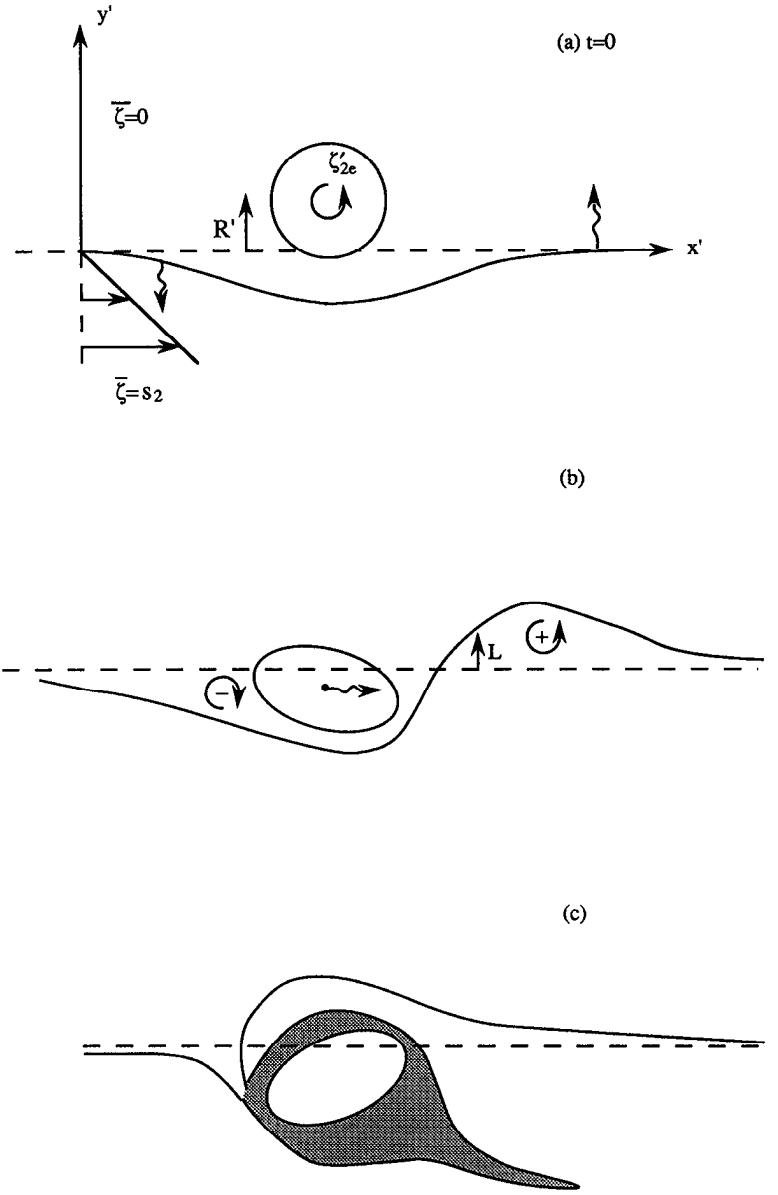

Figure 1. Schematic diagram of pure barotropic entrainment (after Stern, 1991). (a) An initially circular eddy of vorticity ζ'_{2e} with its center at $y' = R'$ interacts with a semi-infinite shear layer of piecewise uniform vorticity $(0, s_2)$. The wiggly arrows indicate the transverse velocity induced on the interface (solid curve). (b) The resulting interfacial deflection L bounds clockwise (+) vorticity anomalies downstream and negative ones upstream. These cause the eddy controid to move into the shear flow. (c) The clockwise winding of L results in the entrainment of the eddy and its surrounding irrotational fluid (stipled) inside a "new" shear flow interface (see text).

contains a circular eddy with vorticity $\zeta'_{2e} > 0$ and strength

$$\Omega' = \int\int \zeta'_{2e}\, dx'\, dy',$$

with its center at some "relatively small" distance $y' = R'$. The eddy circulation perturbs L, and thereby induces vorticity anomalies (denoted by + and −), as defined by the difference between the actual vorticity and the undisturbed flow vorticity at any point. These anomalies determine the total *transverse* velocities, which cause the centroid of the eddy to move closer to the shear flow (Fig. 1b). This motion will increase both the interfacial deflection and the total amount of the vorticity anomalies subtended by L, thereby augmenting the motion of the eddy toward $y' < 0$. As this occurs the eddy circulation causes the downstream branch of L to wind counterclockwise around the eddy until *close contact* is made (at time t_f) with the upstream L-branch, thereby "virtually" (e.g., Fig. 1c) encircling the eddy and some of its surrounding ($\bar{\zeta} = 0$) fluid. This means that an essentially multi-connected L-curve tends to form, as is made explicit by "cutting and reconnecting (four) ends" (S91, SB) at the close contact point. One of the two simply connected L-curves so formed extends from $x' = -\infty$ to $x' = +\infty$, and this defines a "new" shear flow interface; on one side of this there is only irrotational fluid, and on the other side is the second L-curve, which is closed and contains both the Ω' eddy and its surrounding $\bar{\zeta} = 0$ fluid. Their combined areas A' measures the net mass transfer across the new interface and into the stream, where it will eventually be mixed and advected downstream, thereby increasing the total stream transport. The value of A' depends on s_2, Ω', R' and on the initial geometry. It was found (S91) that if R' is *not* large compared to the "natural' length scale $(\Omega'/s_2)^{1/2}$, and if $\zeta'_{2e} > s_2$ is not too large then the entrained area scales as

$$A' \sim \frac{\Omega'}{s_2}. \tag{1.1}$$

The large R' case, on the other hand, leads to a weak (linear theory) eddy-shear flow interaction (Stern and Flierl, 1987) in which the distant vortex is not entrained. Likewise, the $\zeta'_{2e}/s_2 \gg 1$ case corresponds to a dynamically passive shear flow whose interface is merely wound around a nondisplaced eddy.

A qualitatively similar entrainment process occurs in the 1½ layer model (SB), where piecewise uniform potential vorticity domains replace the piecewise uniform vorticity regions of the barotropic problem. In both cases the contour dynamical procedure (Meacham, 1991) is used in the numerical calculation of the nonlinear evolution. These relatively simple models (compared to spectral calculations) reduce the number of degrees of freedom, thereby facilitating understanding, and allowing quantitative exploration of a greater parametric range.

The effects in both of the previously cited studies will appear in the two layer case (Fig. 2), where the lower layer has finite mean depth H_2 and a basic velocity $\bar{U}_2(y')$.

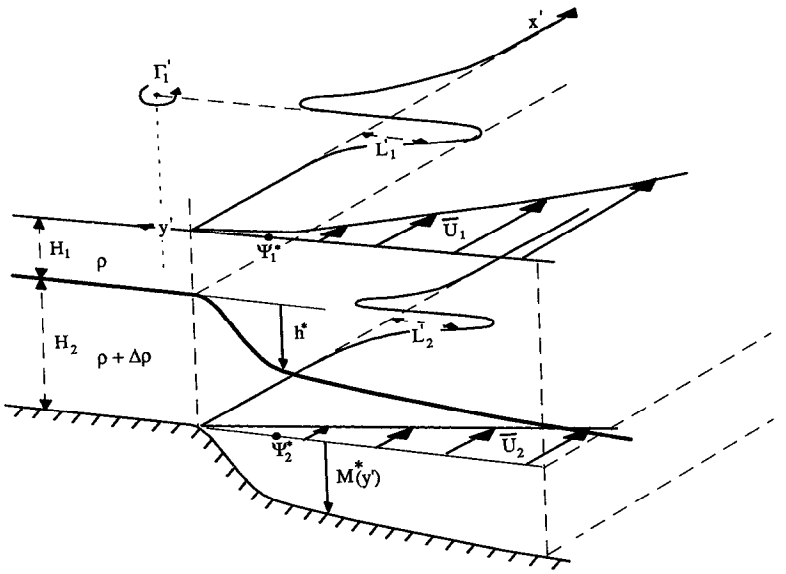

Figure 2. Perspective sketch of a two layer model with undisturbed velocities $\overline{U}_1(y')$, $\overline{U}_2(y')$ in the upper and lower layers respectively. ψ_1^*, ψ_2^*, are the respective dynamic pressures and h^* is the downward displacement of the density interface. Piecewise uniform potential vorticity is achieved by choosing the bottom topography M^* such that the undisturbed lower layer thickness is uniform. This basic state is disturbed by piecewise uniform potential vorticity eddies, but for clarity only an upper layer point vortex (strength Γ_1') is shown. The eddies induce transverse displacements L_1', L_2' of the potential vorticity interfaces.

In order to achieve the simplification of a piecewise uniform potential vorticity model we will consider the particular bottom topography

$$M^*(y') = \overline{h}^*(y'). \tag{1.2}$$

Although this is somewhat artificial, it does correspond to the oceanographically relevant case of a deep isopycnal layer having nearly constant thickness. This bottom layer will then have piecewise uniform potential vorticity if $\overline{U}_2(y')$ has piecewise uniform shear, and piecewise uniform potential vorticity in the upper layer will be achieved by choosing appropriate values of $H_1 + \overline{h}^*$, $\overline{U}_1(y')$, as will be seen. In addition, the upper and lower layers will contain eddies of piecewise uniform vorticity whose integrated values define the respective strengths Γ_1', Γ_2', but for clarity only (part of) an upper eddy is shown in Figure 2.

2. Two layer equations and the deep bottom layer limit

As in SB, the quasi-geostrophic potential vorticity ω^* of an isopycnal layer of mean thickness H_m is defined by $\omega^* = \zeta^*/f - h^*/H_m$ where $h^*(x', y', t')$ is the deviation of the layer of thickness from H_m, f is the (constant) Coriolis parameter, $\zeta^* = f^{-1}\nabla^2\psi^*$ is

the relative vorticity expressed in terms of the dynamic pressure ψ^*, and $f^{-1}(-\partial\psi^*/\partial y', \partial\psi^*/\partial x')$ are the (x', y') velocity components. If subscript "1" denotes the upper layer of density ρ, and "2" denotes the lower layer of density $\rho + \Delta\rho$, then $\nabla\psi_1^* = \nabla\psi_2^* + g^*h^*$ is the hydrostatic relation ($g^* = g\Delta\rho/\rho$), and

$$\omega_1^* = f^{-2}\nabla^2\psi_1 - h^*/H_1,$$

$$\omega_2^* = f^{-2}\nabla^2\psi_2 + (h^* - M^*)/H_2,$$

are the piecewise uniform fields of conservative potential vorticity. When the corresponding equations for the undisturbed fields $\bar{\omega}_1$, $\bar{\omega}_2$ are subtracted from the total fields, we obtain equations for the piecewise uniform residual fields ω_1', ω_2' as functions of the disturbance fields ψ_1', ψ_2', h'. The well known diagnostic equations for the barotropic component $H_1\psi_1' + H_2\psi_2'$ and the baroclinic component $\psi_1' - \psi_2'$, obtained by linear combination of the ω_1', ω_2' equations, are

$$\nabla^2(H_1\psi_1' + H_2\psi_2') = f^2(H_2\omega_2' + H_1\omega_1'), \tag{2.1}$$

$$(\nabla^2 - 1/\lambda^2)(\psi_1' - \psi_2') = -f^2(\omega_2' - \omega_1'), \tag{2.2}$$

$$\lambda = (g^*/f^2)^{1/2}(1/H_1 + 1/H_2)^{-1/2}. \tag{2.3}$$

The residual ω_i' are composed of two parts, one of which is due to the eddy strength defined by

$$\Gamma_i' = \int\int (\omega_i')_{\text{eddy}}^{dx'dy'}$$

and the second is the interfacial potential vorticity anomaly which depends only on the transverse deflection L_i' of the interface and on $\bar{\omega}_i$ in the layer i. The Lagrangian velocity $(dx_i'/dt, dL_i'/dt)$ at each point (x_i', L_i') on the L_i' interface is obtained by solving the inhomogeneous equations (2.1)–(2.2) for $f^{-1}(-\partial\psi_i'/\partial y', \partial\psi_i'/\partial x')$, evaluating these components on the L_i' interfaces, and adding in the basic velocity $(\overline{U_i}, 0)$. Each of the points used to discretize L_i' is then moved with this velocity in one time step, and iteration then gives $L_i'(x_i', t)$.

The Green's function for solving the Poisson equation (2.1) is logarithmic, and the Green's function for Eq. (2.2) is the Bessel function (K_0). By adding and subtracting the (integral) solutions for $H_1\psi_1' + H_2\psi_2'$ and $\psi_1' - \psi_2'$ we obtain the individual pressure disturbances:

$$\psi_1' = \frac{f^2}{2\pi(1+\epsilon)}\int\int d\xi\, d\eta \left((\omega_2' + \epsilon\omega_1')\ln\left(\frac{R}{R_0'}\right) + (\omega_2' - \omega_1')K_0\left(\frac{R}{\lambda}\right)\right), \tag{2.4}$$

$$\psi_2' = \frac{f^2}{2\pi(1+\epsilon)}\int\int d\xi\, d\eta \left((\omega_2' + \epsilon\omega_1')\ln\left(\frac{R}{R_0'}\right) - \epsilon(\omega_2' - \omega_1')K_0\left(\frac{R}{\lambda}\right)\right), \tag{2.5}$$

where

$$R = [(x' - \xi)^2 + (y' - \eta)^2]^{1/2}, \qquad \epsilon = \frac{H_1}{H_2}, \tag{2.6}$$

and where the normalizing constant R_0' may be chosen as convenient (see below). Note that the upper layer anomalies ($\omega_1' d\xi d\eta$) in (2.5) must be integrated over all (x', y') in the *upper* layer to obtain their contribution to the *lower* layer ψ_2', whereas the $\omega_2' d\xi d\eta$ terms are to be integrated over the *lower* layer in (2.5); likewise for the integrations in (2.4).

Before turning to the numerical calculations, some simple but important properties of (2.4)–(2.5) will be noted for the asymptotic limit

$$\epsilon = \frac{H_1}{H_2} \ll 1,$$

and for the case in which *only a lower layer eddy* $\Gamma_2' > 0$ (i.e. $\Gamma_1' = 0$) is present to disturb the basic flow with fixed

$$s_i = -dU_i/dy \text{ at } y = 0^-, \tag{2.7a}$$

$$s = s_1 - s_2. \tag{2.7b}$$

Then the $\epsilon \to 0$ limit of (2.5) is

$$\psi_2' = \frac{f^2}{2\pi} \int\int d\xi\, d\eta\, \omega_2' \ln \{[(x' - \xi)^2 + (y' - \eta)^2]^{1/2} (R_0')^{-1}\}, \tag{2.8}$$

where R_0' may be taken as the initial centroid ordinate of the eddy. Because (2.8) is independent of the perturbations it induces in the upper layer, the asymptotic contour dynamical equations for $L_2'(x', t')$ are the same as for an analogous pure barotropic problem (S91), and thus *the entrained area A' should be independent of s_1*. The importance of this conclusion lies in the fact that in the limit of large H_2, a finite A' implies a large entrained volume $H_2 A'$ in the two layer problem.

Since an increase in s_1 increases the $|\omega_1'|$ associated with the L_1' deflection, the question arises as to whether the $\epsilon\omega_1'$ terms in (2.5) are negligible, and whether the $\epsilon \to 0$ limit is valid when s_1 is large (with fixed s_2, Γ_2'). But the increase of s_1 also increases the intrinsic restoring force on the interface, so that the area occupied by the ω_1' anomalies decreases, thereby offsetting the increase in $|\omega_1'|$. In order to show that the integrated effect of $|\omega_1'|$ yield velocities independent of $s_1 \to \infty$ we develop the following scale analysis to obtain asymptotic equations when $\epsilon \to 0$, $s_1 \to \infty$. Let the lower layer s_2^{-1} be the time scale, $(f\Gamma_2'/s_2)^{1/2}$ the "natural" length scale, and $L_1 \equiv Q/s_1$ the upper interface deflection, where Q is independent of $s_1 \to \infty$. Thus the y' interval over which the $\omega_1' \sim s_1$ are integrated is $\int d\eta \sim L_1 \sim Q/s_1$, and

consequently $\int \omega_1' \, d\eta \sim Q$ is independent of s_1. The net contribution of ω_1' to Eq. (2.5) is then uniformly $O(\epsilon) \to 0$, so that (2.8) holds, and L_2 is indeed independent of $s_1 \to \infty$. The asymptotic equation for Q is obtained by noting that $dL_1/dt \sim s_1^{-1} \to 0$, and therefore $\partial\psi_1'/\partial x' \to 0$ on $y' = L_1 \sim s_1^{-1} \to 0$. By collecting terms in (2.4) which are independent of ($s_1 \to \infty$, $\epsilon \to 0$), we find one group coming from the $\omega_2' d\xi d\eta$ terms, which involve only the aforementioned L_2 anomalies and the *lower* layer Γ_2'. The remaining contributor to (2.4) and to $\partial\psi_1'/\partial x' = 0$ is $\int\int K_0 \omega_1' d\xi d\eta \sim \int K_0(s_1 d\xi) Q/s_1$ which is also independent of s_1, and which requires an x-integration over the $Q(x, t)$ contour. The resulting asymptotic balance for the upper interface is an inhomogeneous integral equation for Q, which corresponds to a quasi-static response to the independently determined evolution of L_2 and the lower layer eddy. We must note, however, that this analysis implicitly assumes a *stable* undisturbed state, for otherwise the small eddy induced $L_1 \sim 1/s_1$ might amplify on the relatively fast time of a baroclinic instability. These inferences will be useful in organizing the numerical results which follow.

For the finite values of (ϵ, s_1) used in the numerical calculations of (2.4)–(2.5) the non-dimensionalization will employ λ as the length scale (except as otherwise noted), and s^{-1} (2.7b) as the time scale. Then the non-dimensional baroclinic shear at $y = 0^-$ in the basic state is unity, and the corresponding non-dimensional shear of the lower layer is

$$r_s = s_2/s. \tag{2.9}$$

The corresponding non-dimensional potential vorticity anomalies are denoted by $\omega_i = \omega_i'(s/f)^{-1}$, the nondimensional area is $A = A'/\lambda^2$, and the non-dimensional strength Γ_2 of the eddy in the lower layer is related to the previous value (Γ_2') by

$$\Gamma_2' = \lambda^2(s/f) \int\int \omega_{2e} \, dxdy = \lambda^2(s/f)\Gamma_2. \tag{2.10}$$

The asymptotic result (2.8) suggests that for fixed geometry (e.g. radius and location of the initial lower layer eddy) the dimensional entrained area A' should be proportional to the pure barotropic value (1.1). Since $\zeta_{2e}' = f\omega_{2e}'$ when $H_2 \to \infty$ Eq. (1.1) yields

$$A' \sim s_2^{-1} \int\int f\omega_{2e}' \, dx'dy' = f\Gamma_2'/s_2,$$

and when this is converted to non-dimensional units, using $A' = A\lambda^2$ and (2.10), we get the suggested asymptotic *scaling* relation

$$A \sim s\Gamma_2/s_2 = \Gamma_2/r_s. \tag{2.11}$$

How do the following two-layer calculations for *finite* ϵ, r_s compare with this?

3. Numerical results and discussion

In the numerical calculations x-periodic boundary conditions with a (sufficiently) large wavelength are used, in which case the logarithmic Green's function in (2.4)–(2.5) is replaced by the well known formula for a periodic barotropic vortex array; the periodic K_0 array is, however, approximated by the sum over a finite number of wavelengths. This procedure, as well as other aspects of the implementation of the contour dynamical method is the same as in SB.

For the case of the semi-infinite *shear layer* (Fig. 2) with piecewise uniform potential vorticity, the non-dimensional basic velocity profiles are

$$\bar{u}_1(y) = \begin{cases} 0 & y > 0 \\ -\mu^{-1} \sinh(\mu y) - r_s y & y < 0, \end{cases} \tag{3.1}$$

$$\bar{u}_2(y) = \begin{cases} 0 & y > 0 \\ -r_s y & y < 0, \end{cases} \tag{3.2}$$

$$\mu = (1 + \epsilon)^{-1/2}, \tag{3.3}$$

and the nondimensional Eqs. (2.1)–(2.2) are

$$\nabla^2(\epsilon\psi_1 + \psi_2) = \epsilon\omega_1 + \omega_2, \tag{3.4a}$$

$$(\nabla^2 - 1)(\psi_1 - \psi_2) = \omega_1 - \omega_2. \tag{3.4b}$$

If (L_1, L_2) denote the non-dimensional deflections of the shear flow interfaces, and ω_{1e}, ω_{2e} denote the uniform eddy potential vorticities of strength Γ_1, Γ_2, then

$$\omega_1 = \omega_{1e} + \begin{cases} 1 + r_s & 0 < y < L_1 \\ -(1 + r_s) & 0 > y > L_1 \\ 0 & \text{otherwise,} \end{cases} \tag{3.5}$$

$$\omega_2 = \omega_{2e} + \begin{cases} r_s & 0 < y < L_2 \\ -r_s & 0 > y > L_2 \\ 0 & \text{otherwise,} \end{cases} \tag{3.6}$$

where the bracketed quantity gives the anomaly due to the interfacial deflection. For the case of a baroclinic *jet*, Eqs. (3.1) and (3.5) are respectively replaced by

$$\bar{u}_1(y) = \begin{cases} \dfrac{1}{2\mu} e^{-\mu y} & y > 0 \\ \dfrac{1}{2\mu} e^{\mu y} - r_s y & y < 0, \end{cases} \tag{3.7}$$

$$\omega_1 = \omega_{1e} + \begin{cases} r_s - 1 & 0 < y < L_1 \\ -(r_s - 1) & 0 > y > L_1, \end{cases} \tag{3.8}$$

and $\bar{u}_2$, ω_2 are unchanged. Most of the following calculations, however, are for the shear layer (3.1).

Consider first the case of a *point* potential vortex with $\Gamma_2 > 0$ (and $\Gamma_1 = 0$) located initially at $y_e(0) = 0.2$ in a lower layer with everywhere vanishing potential vorticity gradient ($\bar{u}_2(y) \equiv 0, r_s = 0$). The L_2-curve then merely provides a passive *tracer* for Lagrangian parcels advected directly by Γ_2, and indirectly by the upper layer vortex anomalies associated with L_1. It appears (Fig. 3a) from the contour dynamical calculations that the latter are so small for $\epsilon = .5$, $\Gamma_2 = 1$ that their induced lower layer velocities hardly change the vortex position ($y_e(26)$), so that it is not entrained *under* the shear flow. A merely kinematic response occurs in the lower layer, as the L_2-tracer is wound around the vortex (Fig. 3a) by its own circulation.

When s_2 is finite (Fig. 3b), on the other hand, the L_2-deflection induced by the eddy produces positive (negative) potential vorticity anomalies downstream (upstream) from $y_e(t)$, and both anomalies produce a lower layer velocity which causes $y_e(t)$ to decrease. (These effects are analogous to those described for Fig. 1.) The approach of the vortex to L_2 then increases the latter deflection, thereby increasing both the total vorticity anomalies and their effect in decreasing $y_e(t)$. Eventually (Fig. 3b) the point vortex enters the lower layer shear region ($y < 0$), and the continued counterclockwise winding of L_2 results in a "close contact" (at $x \sim -.5$) of the original downstream branch of L_2 with its upstream branch. By "cutting and reconnecting" (as previously mentioned) a new shear flow interface is formed, inside of which is the vortex and its surrounding low potential vorticity fluid (unstipled). The total entrained area A represents a net transfer of mass across the *new* interface of the mean shear flow in the lower layer.

When the run in Figure 3a was repeated with the lower vortex transferred to the upper layer (i.e. $\Gamma_1 > 0, \Gamma_2 = 0, r_s = 0$), entrainment occurred across the *upper* layer interface (not shown), in a manner dynamically similar to that which occurs in the 1½ layer model (SB), and the passive L_2-curve was merely wound in a spiral about a stationary central point. In a second repetition, using an initially depth independent vortex (i.e. $\Gamma_1 = \Gamma_2 > 0$) at $y = 0.2$, and $s_2 = 0$, the upper ($\Gamma_1 > 0$) vortex interacted with L_1 as occurred previously (for $\Gamma_2 = 0$), but the lower layer vortex (Γ_2) remained near $y = 0.2$, and merely wound L_2 around it; i.e. the depth dependent vortex split and entrainment occurred in the upper layer but not in the lower one. These results indicate that, in addition to a bottom eddy ($\Gamma_2 \neq 0$), a bottom layer potential vorticity gradient ($s_2 \neq 0$) is necessary for a net mass transfer underneath the surface current.

Next to be considered are finite area bottom eddies, or more generic fluctuations of potential vorticity, such as a "patch" (Fig. 4) which is in close contact with the edge of the stream. In addition to the computational efficiency (cf. SB) provided by such a

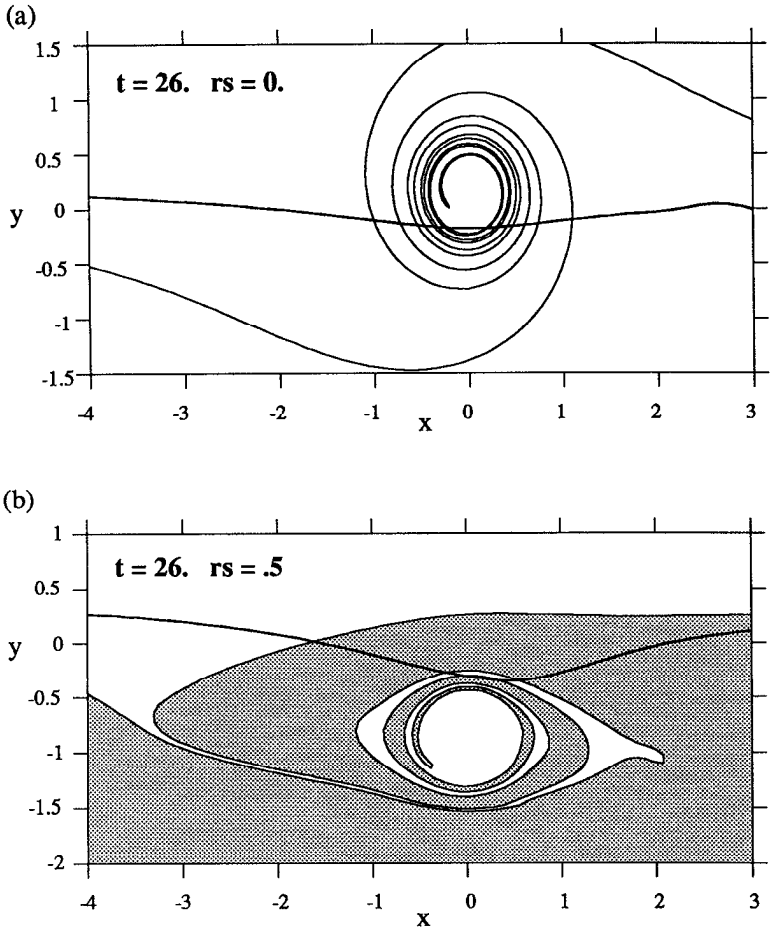

Figure 3. The interfacial deflections L_1, L_2 at $t = 26$ produced by a lower layer ($\epsilon = 0.2$) point vortex of non-dimensional strength $\Gamma_2 = 1$, initially at $y_e(0) = 0.2$. The $x = 0$ origin moves with the vortex center in all that follows. (a) No lower layer shear flow ($s_2 = 0$). The L_2-curve is merely wound around the vortex center whose position $y_e(26) = .16$ is almost unchanged. The nearly horizontal curve is L_1. (b) Same as (a) except that a lower layer shear flow ($r_s = .5$) has been added. This results in $y_e(26) = -.86$, and an entrainment of irrotational (unstipled) fluid inside the shear flow (stipled). The deflection of the upper layer curve is larger than in (a).

structure (as compared with an eddy *separated* from the interface), it might fairly represent part of a complex eddy field which is near the stream at a certain time; our model attempts to isolate a subsequent interaction with the stream which leads to entrainment. In all the following runs, $\Gamma_1 = 0$, and the semi-circular patch radius was chosen so that its initial centroid was at the same ordinate $y_e(0) = 0.2$ as in the runs using point vortices. Except for the smaller $\Gamma_2 = .5$, the parameters used in Figure 4

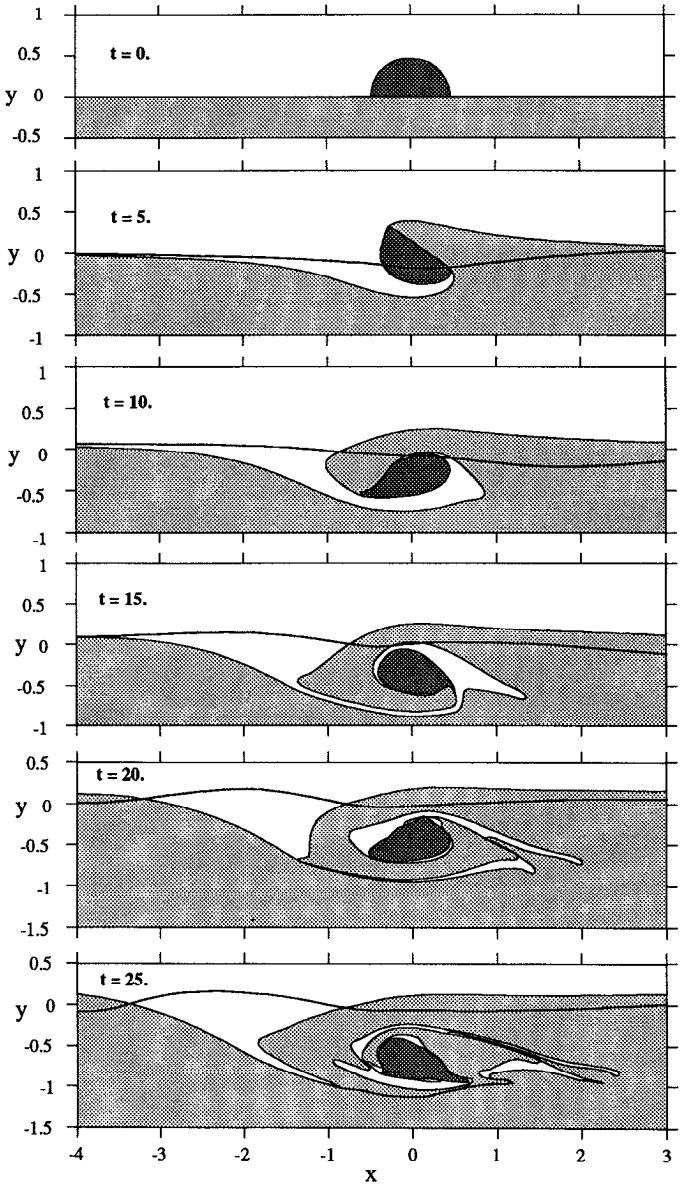

Figure 4. A semi-circular patch (cyclonic "eddy") of radius 0.471 ($y_e(0) = 0.2$), potential vorticity = 1.43, and strength $\Gamma_2 = 0.5$ is initially in close contact with $L_2(x, 0) = 0$, when $r_s = .5$, $\epsilon = .2$, $\Gamma_1 = 0$. At $t = 20$ the eddy and its surrounding (unshaded) fluid are entrained inside the "new" interface formed by cutting L_2 at $x \sim -1.75$ (see text). The nearly horizontal curve is the slightly deflected L_1-interface.

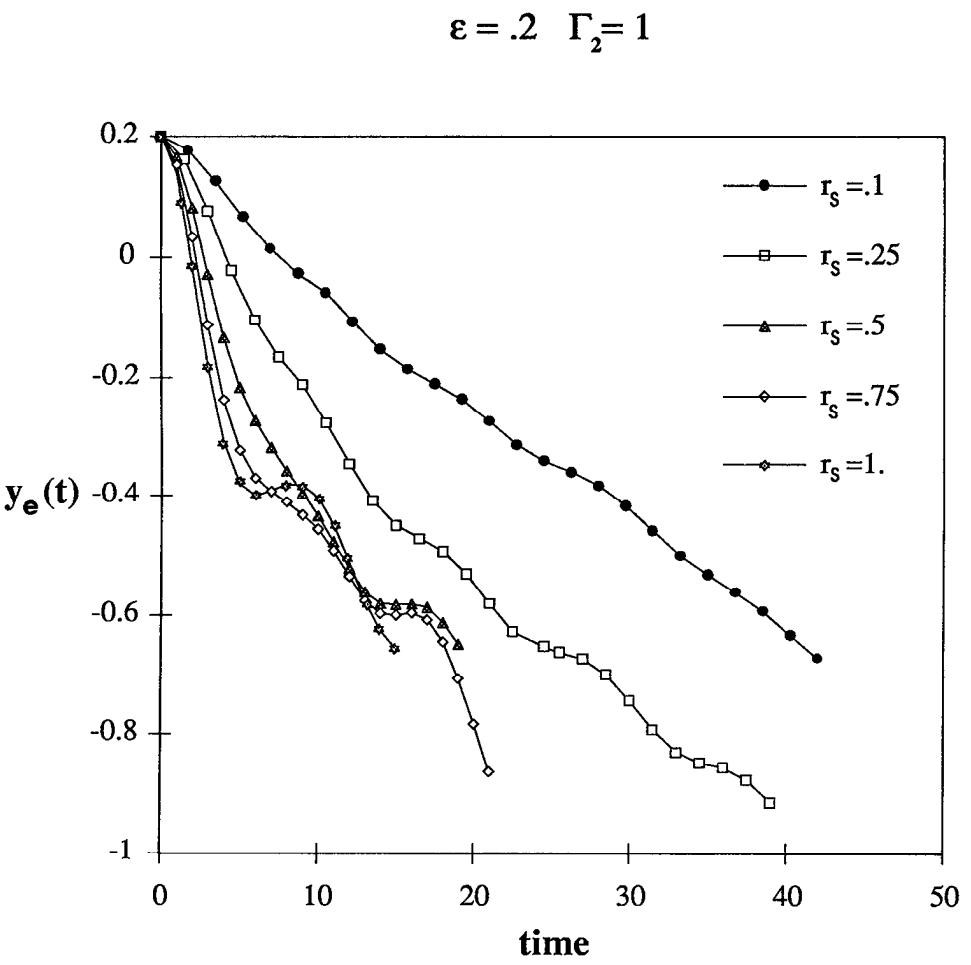

Figure 5. Time variation of the centroid of initially semi-circular eddies with radius 0.471 ($y_c(0) = 0.2$). (a) $\Gamma_2 = 1$, $\epsilon = 0.2$. (b) $r_s = .5$, $\epsilon = 0.2$. (c) $r_s = .5$, $\epsilon = 1$. The entrainment of the eddy is clearly implied in Figure 5a by its rapid motion into the region ($y < 0$) occupied by the shear flow.

are the same as for the point vortex used in Figure 3b. The lower layer vorticity anomalies, induced by the eddy at $t = 5$ causes it to move into the shear layer at $t = 10$, and the winding of L_2 results in complete entrainment of the eddy at $t = 25$; but the deflection of the upper layer interface is notably small.

The large number of runs summarized in Figure 5 indicate the way the entrainment depends on the parameters; e.g., increasing r_s (Fig. 5a) decreases the time it takes for an eddy and its surrounding water mass to pass from the outside to the inside of the lower layer interface. It should be mentioned that in the runs with very small r_s (e.g., $r_s = 0.1$) the L_2 plot (not shown) contains *many* spiral windings of the

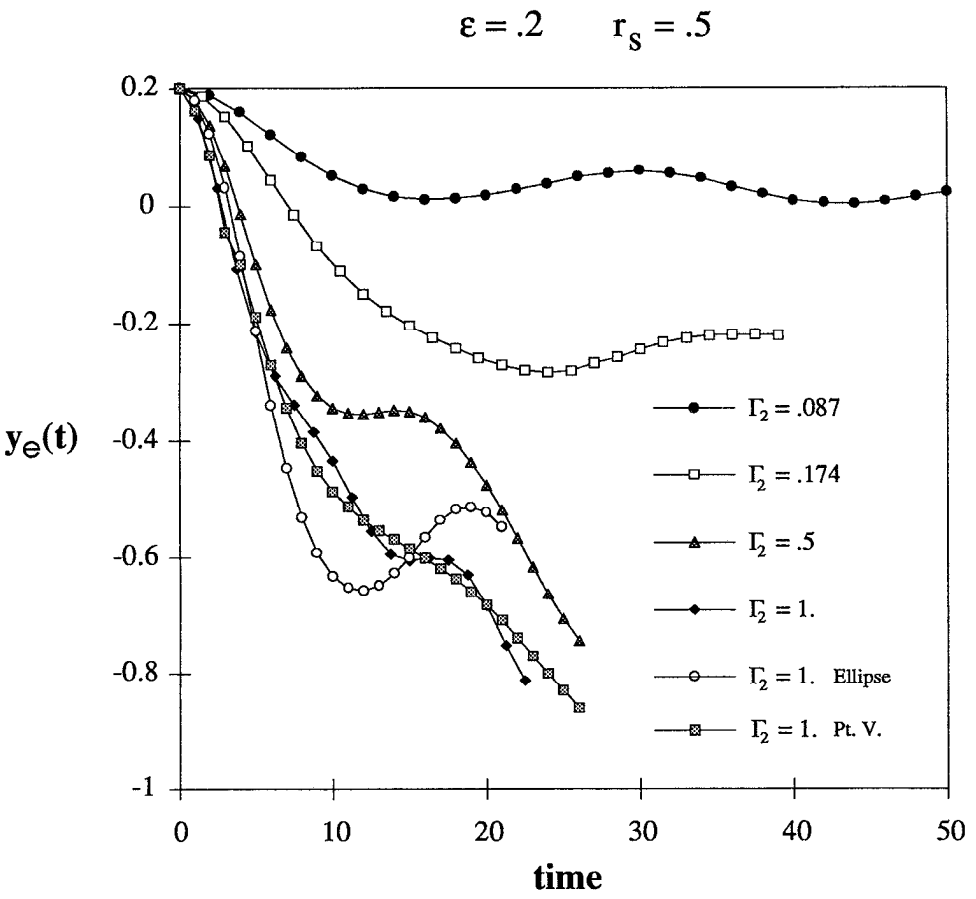

Figure 5. (Continued)

interface around the eddy before "close contact" and definitive entrainment occur; this greatly increases the number of Lagrangian points and otherwise causes problems in resolving the windings. For this reason smaller r_s values were not considered, and when $r_s \to 0$ the nonentraining regime, typified by $s_2 = 0$ (cf. Fig. 3a), is approached. Figure 5b suggests that for fixed ϵ, r_s there is a critical value of Γ_2 below which entrainment also does not occur [see the small L_1 amplitude (linear) calculation of Stern and Flierl (1987) when $\Gamma_2 \to 0$]. There also appears to be little difference in the displacement of a point vortex, a semi-circle, and a semi-ellipse with the same $\Gamma_2 = 1$. Figure 5c shows that the rate of entrainment of a $\Gamma_2 = 1$ eddy does not differ much from that for the smaller ϵ in Figure 5b, indicating a rapid approach to the asymptotic ($\epsilon \to 0$) theory.

The entrained area for a shear layer interacting with a semi-circular eddy of fixed strength $\Gamma_2 = 1$ is plotted in Figure 6 as a function of r_s for $\epsilon = 0.2$. (The curve should

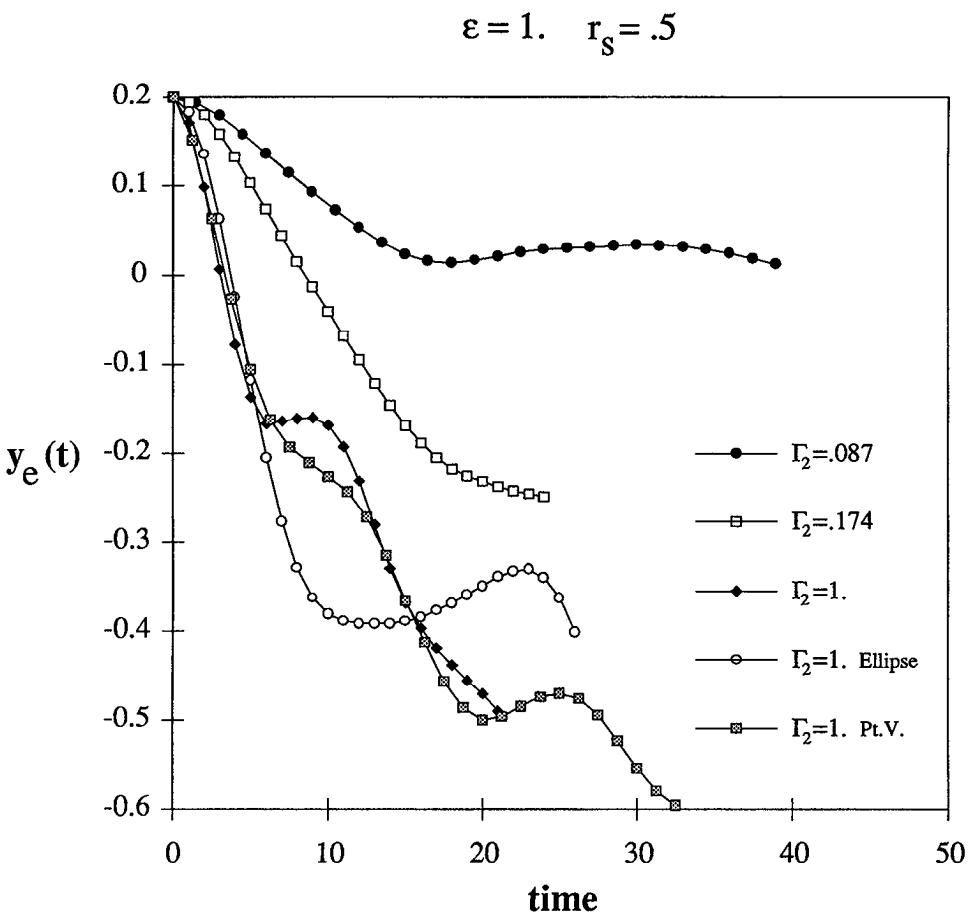

Figure 5. (Continued)

not be extrapolated to $r_s < 0.1$, for reasons mentioned previously in connection with Figure 5a, viz no entrainment occurs for much smaller r_s when Γ_2 is held constant.) The second set of points in this figure will be discussed subsequently. All of our two-layer entrainment runs are plotted in Figure 8 using the barotropic scaling (2.11) of the asymptotic theory. It is noteworthy that this collapses all of the runs, covering a large range of (ϵ, r_s), into a single (nearly linear) curve. These baroclinic results were also compared with a *pure* barotropic one in which $\epsilon = 0$ (in Eq. 2.5), and for which A is independent of r_s. In this run we set $r_s = 1$, which makes s_2^{-1} the time scale, and calculated A for each Γ, using an initially semicircular barotropic eddy with centroid at $y_e(0) = 0.2$. The computed value of A for each $\Gamma/r_s = \Gamma/1$ was entered in Figure 8 and, as expected, the pure barotropic points overlap those for other values of r_s, ϵ.

Further verification of the dominant barotropic effect was obtained by changing the upper mean field from a shear layer (3.5) to a jet (3.7), for which the difference in

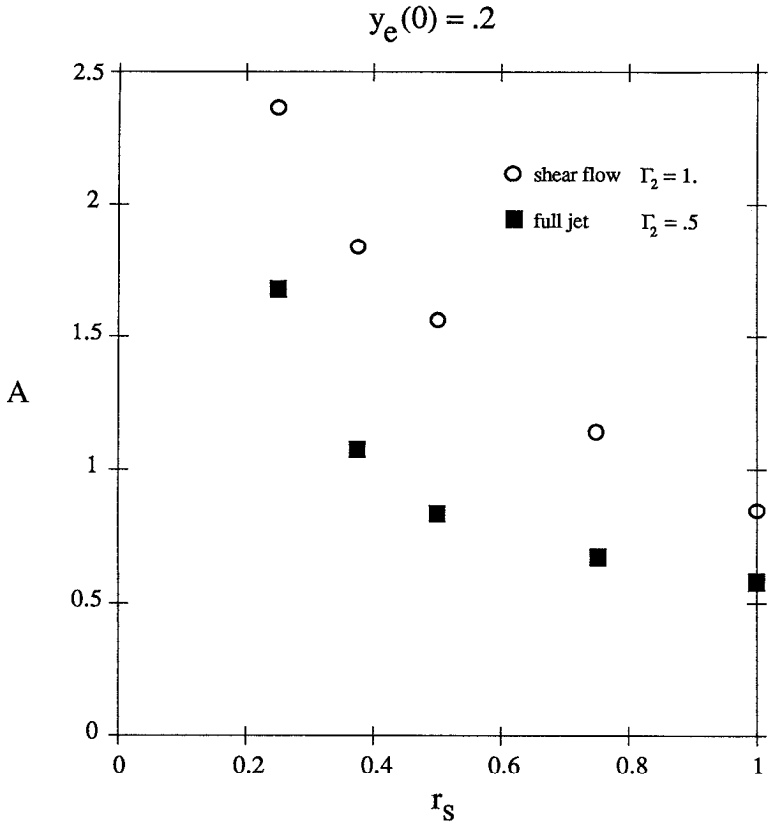

Figure 6. Nondimensional entrained area (A) produced by semi-circular bottom eddy as a function of r_s for $\epsilon = 0.2$, $y_e(0) = 0.2$. The open symbols are for an upper layer shear flow (Eq. 3.1) when $\Gamma_2 = 1$, and the solid symbols are for an upper layer jet (3.7) when $\Gamma_2 = .5$.

undisturbed lower layer shear across $y = 0$, as well as the values of $(\epsilon, y_0, \Gamma_2)$, are the same as for the shear layer in Figure 4; but the difference in baroclinic shear across $y = 0$ has an opposite *sign* in the two cases. The computed A is the same in both cases, and the main difference is the larger L_1 amplitude in the jet problem (Fig. 7). This is attributed to a baroclinic instability, since the upper and lower layers of the jet model have oppositely directed potential vorticity gradients [see the remark at the end of the scale analysis in the paragraph preceeding Eq. (2.9)]. Figure 6 compares the variation of A with r_s for this jet and for the shear layer. Figure 8 shows that both sets of points lie on the same normalized curve, thereby verifying that for $\epsilon = .2$ the upper layer does not affect the entrained area in the lower layer.

4. Conclusion and suggestions

A simple scale analysis was used to show that the entrainment of a lower layer eddy into a shear flow depends mainly on the deep layer, and not on the stronger potential

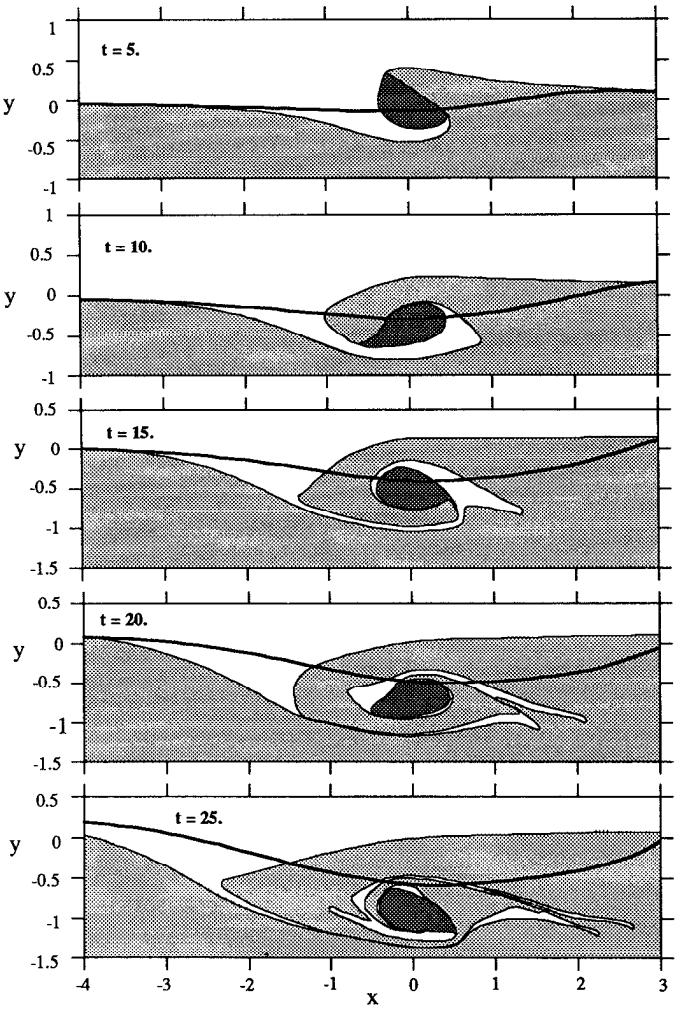

Figure 7. Same as Figure 4 except that the undisturbed baroclinic flow is a jet (3.7) with its maximum velocity on $y = 0$.

vorticity gradients in the thin overlying layer. The scaling relation (2.11) for total entrained area was numerically verified (Fig. 8) not only for small H_1/H_2, but also for a larger range of two layer parameters in an ensemble (Fig. 8) consisting of a bottom eddy which is initially near the edge of the lower shear layer. The somewhat artificial topography (Eq. 1.2) used to achieve model simplification restricts our entrainment calculations to a deep isopycnal layer of *uniform* thickness.

The oceanographic significance of the finite entrained area A' in the large H_2 limit is due to the large entrained *volume*. This represents a potentially significant addition to the transport of the thin and fast upper layer of the Gulf Stream, assuming that the

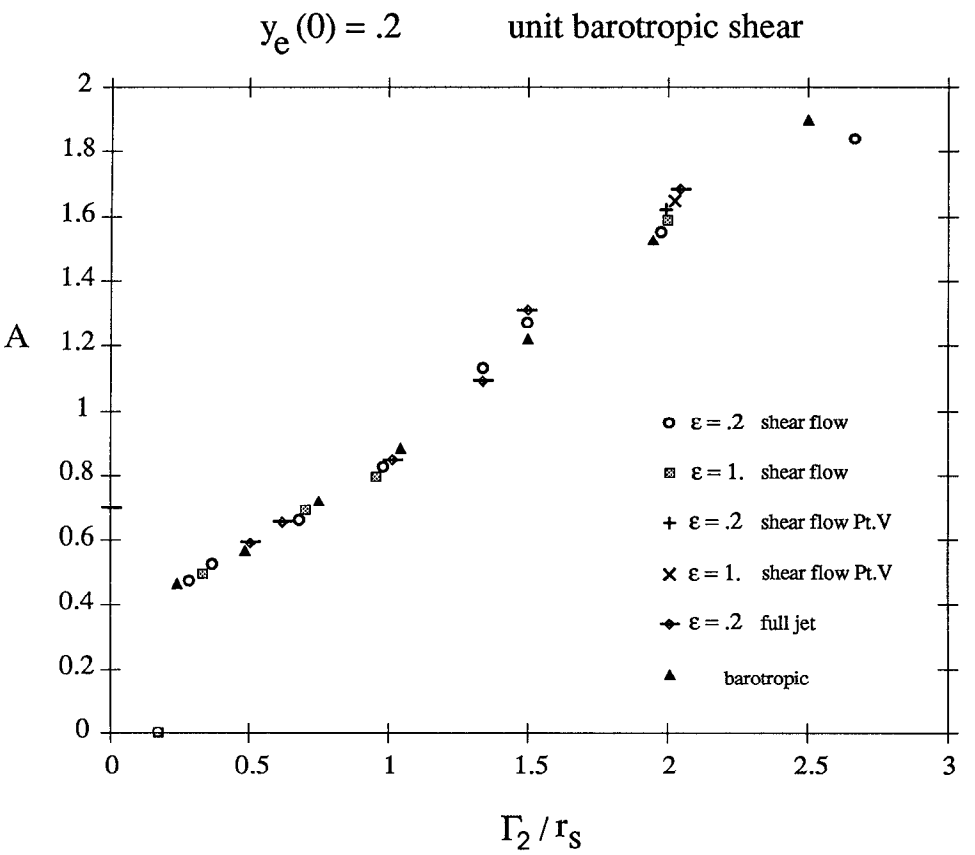

Figure 8. Summary of non-dimensional area (A) entrained in the bottom layer as a function of the scale (Γ_2/r_s) suggested by the asymptotic theory. All runs have $\Gamma_1 = 0$ and the same initial value for the center of the bottom layer eddy. These runs include the point vortex, the semi-circular eddy, and a corresponding *pure* barotropic eddy (see text). The points labeled "full jet" are for Eq. (3.7), and the others are for Eq. (3.1). The collapse of these points onto a single curve indicates that entrainment in the bottom layer depends mainly on the strength of the eddy therein and on the lower layer shear; independent of the upper layer current.

entire entrainment event (e.g. Figs. 4 and 7) is *repeated* intermittently in space-time, as successive patches of eddy potential vorticity are advected toward the stream's edge by a broad mean current ("gyre") on either side of the deep Gulf Stream.

These suggestions may be elucidated in the context of the simple barotropic model (Fig. 1). Suppose the shear flow interface is initially undisturbed ($L(x, 0) = 0$), and at some distance R' outside this there is a *compact* eddy having equal and opposite amounts of vorticity in an inner core and in an outer annular shell (respectively), so that *no* velocity is induced on L. Now add a steady weak mean flow directed toward the shear flow interface; e.g. by inserting a *fixed* vortex at some distant point (as was done in SB Sec. 3). The velocity produced by this weak mean field will cause the

compact eddy to move slowly toward the shear flow, and eventually to interact with it. The outer vortical shell will then be advected downstream faster than the core, thereby tending to separate the regions of positive and negative eddy vorticity into two "patches" in close contact with $L(x, t)$. As in the case of Figure 1c, the subsequent interaction may result in the entrainment of the patch whose vorticity is of the same sign as the shear flow. The patch with opposite vorticity can be entrained in the basic flow only if the latter contains vorticity of both signs, such as occurs in a *full* jet (for an example see Sec. 5 of SB). In addition to such a calculation we might also consider a model with a staggered array of such compact eddies, which are successively (and independently) advected to the vicinity of the shear flow front, where they (and the ambient irrotational fluid) are successively entrained inside a "new" interface, thereby providing a time averaged downstream increase in *transport* of the fluid at each point along the mean interface.

A simple estimate of the magnitude of this transport can be obtained in terms of a barotropic "entrainment velocity," as computed in S91, Table 4. This is based on the previously mentioned (Sec. 1) interval t_f between the initial time of approach (e.g. Fig. 1a) and the time at which the entrainment (of area A') is "essentially" complete (e.g. Fig. 1c). From the computed (A', t_f) a time averaged entrainment velocity $V_e \equiv A'/(t_f\lambda_e)$ can be obtained, where $\lambda_e = (\Omega'/s_2)^{1/2}$ is the natural length scale determined by s_2 and the eddy strength. On dimensional grounds the time average transport velocity across the current interface is

$$V_e = C(\Omega' s_2)^{1/2} \tag{4.1}$$

where the nondimensional C might depend on ζ'_{2e}/s_2 and on the initial geometry, where ζ'_{2e} is the eddy vorticity. The numerically determined (S91) value of C for an initially circular eddy of radius a in the limited range $a/\lambda_e = (.46, .40, .32)$ for $\zeta'_{2e}/s_2 = (1.5, 2, 3)$ respectively was

$$C = .11 \pm .02. \tag{4.2}$$

We mention that during the interval t_f the eddy was advected approximately two diameters downstream inside the shear flow. Of greatest significance is the fact that the computed momentum flux was directed toward the shear flow ("counter-gradient" flux), so that in addition to incorporating mass the eddy was supplying momentum and energy to the stream.

The major uncertainty in (4.2) is due to the subjective factor in determining the cutoff time t_f. Consequently an independent determination (by JRB) was made for the pure barotropic calculations considered herein. These consisted of an initially semi-circular eddy (centroid at $y_e(0) = 0.2$) in flush contact with the horizontal edge of a shear layer (unit vorticity). For seven values of the eddy strength ($\Omega' = .25, .5, .75, 1.0, 1.5, 2, 2.5$) the value of (4.2) was $C = .081 \pm .001$, and slightly lower (5%)

values were found when the (appropriately normalized) baroclinic runs were included.

Now consider an ensemble of such (separated) eddies located outside the shear flow, and being slowly advected toward its interface by a weak exterior mean flow (the "Recirculation Gyre"). At $t = 0$ the first eddy arrives at the interface and is entrained at $t \sim t_f$. Then the entire process is intermittently repeated in time intervals $O(t_f)$, and also at downstream position intervals of $O(a)$. All the statistical aspects of this ensemble will be parameterized by a single "intermittency factor" γ, so that the mean entrainment velocity at each downstream location is given by

$$\langle V_e \rangle = \gamma(.11)(\Omega' s_2)^{1/2}.$$

Thus in a downstream distance W the total transport through one of the edges bounding the jet is increased by $\langle V_e \rangle W H_2$. For illustrative purpose we take $s_2 =$ 10 cm/sec/50 km, $\Omega' = \pi(30 \text{ km})^2(3s_2)$ and $\gamma = \frac{1}{2}$, thereby obtaining $\langle V_e \rangle =$ 1 cm/sec. Eddies of this size (30 km radius), and r.m.s. velocity $3s_2(30 \text{ km}) = 18$ cm/sec are ubiquitous features (Luyten, 1977) of the deep ocean in the region of the synoptic Gulf Stream.

The suggested generalization for a deep isopycnal layer of nearly uniform thickness is that $\langle V_e \rangle$ is proportional to the product of the maximum mean shear at the edge and the mean eddy strength (integrated potential vorticity).

REFERENCES

Hogg, N. G., R. S. Pickart, R. M. Haudry and W. J. Smethie. 1986. The northern recirculation gyre of the Gulf Stream. Deep-Sea Res., *33,* 1139–1165.

Luyten, J. R. 1977. Scales of motion in the deep Gulf Stream across the continental rise. J. Mar. Res., *35,* 49–74.

Meacham, S. P. 1991. Meander evolution on piecewise-uniform quasi-geostrophic jets. J. Phys. Oceanogr., *21,* 1139–1170.

Stern, M. E. 1991. Entrainment of an eddy at the edge of a jet. J. Fluid Mech., *228,* 343–360.

Stern, M. E. and J-R Bidlot. 1994. Lateral entrainment in baroclinic currents. J. Mar. Res., *52,* 25–53.

Stern, M. E. and G. R. Flierl. 1987. On the interaction of a vortex with a shear flow. J. Geophys. Res., *92,* C10, 10733–10744.

Received: *24 May, 1994;* revised: *11 November, 1994.*